Chemical characterization of $Mg_{0.25}Mn_{0.75}$-H(D) nanocomposites by Atom Probe Tomography (APT)

Abstract

Hydrogen (H)- and deuterium (D)-loaded $Mg_{0.25}Mn_{0.75}$ nanocomposites were prepared by a ball-milling process and Atom Probe Tomography (APT) analyses were carried out in order to investigate the resultant nanostructure. Due to the immiscibility of the Mg−Mn system, non-uniform and interconnected Mg-rich domains with a thickness of several to 10 nm formed in both of the H- and D-loaded composites. Such complex morphology could be attributed to the severe cold-rolling effects induced by ball-milling. The inhomogeneous distribution of D observed by the APT analysis is likely the result of severe lattice distortion and multiple defects, which are cold-rolling effects. While the detection of D in the D-loaded composite was hampered significantly by the desorption of D during specimen preparation, D remained around the boundary of the Mg-rich domains/Mn-rich matrix. This suggests that the modulated intermixing of immiscible Mg and Mn atoms together with the ball-milling effect results in a disordered atomic arrangement around the boundary. This is assumed to be one of the contributing factors in the destabilization of Mg hydride observed in our previous works.

Introduction

The ability to produce hydrogen simply by electrolyzing water using renewable energy makes hydrogen one of the most promising energy carriers in a global sustainable society [1]. In both industrial and urban areas, the demand for safe and compact storage and supply technologies for hydrogen is expected to increase dramatically in the coming decades. Metal hydrides can store hydrogen at moderate pressures, where the volumetric density of hydrogen is higher than gaseous storage compressed up to 70 MPa [2,3]. The high gravimetric storage capacity of Mg, together with low material costs, make Mg one of the most attractive hydrogen storage materials. However, its hydride phase, MgH_2, is so stable that it does not release hydrogen at ambient pressure and temperature, and it is therefore unsuitable for practical stationary and onboard applications. A solution may be to destabilize MgH_2, which is possible by downsizing at the nanometer scale [4–6].

Our group was the first to propose synthesizing nanometer-sized MgH_2 by combining immiscible metals with Mg. In the fabrication of Ti-rich Mg−Ti composites, nanometer-sized MgH_2 clusters coherently embedded in a TiH_2 matrix were formed upon hydrogenation [7]. It has been clearly shown that MgH_2 is destabilized by nanosizing and the extra contribution of the difference in the interface energy between the two metal hydrides [8,9]. Chemical segregation on a nanometer scale accompanies the lattice strain and/or structural change of MgH_2 [10,11], which also contributes to the destabilization of MgH_2 together with the interface energy effect. However, another factor responsible for the stabilization of part of the MgH_2 was the local dissolution of Ti into the Mg domains. Since TiH_2 is more stable than MgH_2, hydrogen atoms occupying the interstitial sites are stabilized by Ti coordination. On this basis, the focus of our research is on a nonhydride forming matrix which is immiscible with Mg.

The Mg−Mn and Mg−Cr nanocomposites synthesized by our group effectively destabilized MgH_2 without any interfering stabilization effect [12,13]. However, the enthalpy for the deuteride dissociation of $Mg_{0.25}Mn_{0.75}$−D powder, at ΔH = 71.5 kJ mol^{-1}−D_2, is not much different from the value of ΔH = 73.1 kJ mol^{-1}−D_2 (ΔH = 74.4 kJ mol^{-1}−H_2) for conventional bulk Mg−D(H) [14]. In an effort to reduce this enthalpy change, we prepared Mg−Mn thin films as *well-mixed* model samples, and found the enthalpy for the hydride dissociation of the fabricated $Mg_{0.30}Mn_{0.70}$−H thin film was as high as ΔH = 46.3 kJ mol^{-1}−H_2 [15]. This indicates the potential of Mg−Mn composites to efficiently destabilize MgH_2. It also opened a new direction in the investigation: the determination and optimization of the mixing status of the immiscible atoms.

In a previous study of the Mg−Mn nanocomposites, Mg domains with a mean size of 10−30 nm were observed by TEM/EDS mapping [12]. However, the composition inside the Mg domains and the spatial extent at even more fine scale remains unknown. Atom Probe Tomography (APT) is suitable for the 3-dimensional investigation of elemental distribution, including light elements like H on a nanometer-scale [16,17]. Some recent publications have reported successful H detection and quantification by the APT [18–21]. Herein, we show the results of the APT analysis on the Mg−Mn nanocomposites loaded with H/D. The complex nanostructured morphology of the Mg−Mn nanocomposites is discussed with the objective of determining the destabilization mechanism of $MgH(D)_2$.

Material and methods

Sample preparation

Mg−Mn nanocomposites were prepared by the ball-milling of MgH_2 and Mn powders with a nominal composition of $Mg_{0.25}Mn_{0.75}$−H. The raw material MgH_2 powder (purity of 98%) and Mn powder (purity of 99.9%) were purchased from Wako Chemical, Co., Ltd. and Furuuchi Chemical Corporation, respectively. Ball milling was performed using stainless steel balls and jars at a speed of 1000 rpm with a ball-to-powder mass ratio of 10:1 for 50 h under an Ar atmosphere using a high-energy vibratory ball mill (Retsch, Emax). The as-milled powder corresponds to the H-loaded specimen. In the case of the D-loaded specimen, the as-milled powder was activated by three deuterium sorption cycles at 523 K which was subsequently deuterated under 1.5 MPa− D_2 at the same temperature for 6 h. Detailed procedures for synthesizing the nanocomposites have been described in our previous reports [12,13]. The $Mg_{0.25}Mn_{0.75}$−H and $Mg_{0.25}Mn_{0.75}$−D specimens were then subjected to APT sample preparation and subsequent analysis, respectively.

Characterization

Both the H- and D-loaded specimens were prepared and analyzed in the same condition. Needle-shaped specimens suitable for APT analysis were prepared from single powder particles by Focused Ion Beam (FIB), with a dual beam SEM/FIB Zeiss Auriga utilizing the standard lift-out and annular milling method on a Si microtip coupon [22]. A typical SEM image of a prepared tip is shown in Figure S1 in supplementary material. For analyzing H species by the APT, O_2-free (ultra-high vacuum, UHV) and/or cryogenic-transfer system to the APT analysis chamber is recommended in order to prevent the discharging (desorption) of once absorbed H/D from the APT specimens [19,23–26]. In this study, however, these recommendations were not followed since the hydrogenation/deuteration of the specimen was conducted before specimen preparation by the FIB. The APT analysis was carried out with a local electrode atom probe (Cameca, LEAP 4000XHR) in laser pulsing mode at 27 K with a pulsed laser energy of 50 pJ and at a pulse frequency of 100 kHz. It has been reported that the extent of the overlap between the signal intensity of H_2^+ and that of D^+ in the mass spectrum depends on the analysis conditions, including specimen temperature, laser energy, pulse repetition rate, and electric field [27–30]. For example, a higher analysis temperature is reported to suppress the H_2^+ signal during the APT laser mode measurement in case of Cu [28]. However, it is also known that such high analysis temperature often disturbs the original D distribution via surface diffusion during the analysis [23]. Therefore, we kept the specimen temperature as low as possible to retain D in the specimen. Reconstruction and data evaluation of the APT results was carried out by the Cameca IVAS 3.6.14 software. In

order to ensure atomic classification, the signal at mass to charge ratio (m/e) = 26 is omitted in the 3D mapping of ions because of the mass peak overlap of $^{52}Cr^{2+}$ (contaminant via ball-milling using stainless steel balls and jars) and $^{26}Mg^{+}$. Since there were sufficiently fewer Cr ions around the Mg rich region than Mg ions, it was possible to locate Mg from the Mn rich matrix in the 3D reconstruction map.

Results and discussion

Figure 1(a) shows a 3D-reconstructed volume of the H-loaded specimen ($Mg_{0.25}Mn_{0.75}$−H) analyzed by the APT. The reconstructed volume shows Mg-enriched domains, with a spatial extent from several to several tens of nm in a Mn-rich matrix. Note that the morphology of these Mg-rich domains is not uniform, as can be clearly seen in Figure 1(b) in the 10 nm-thick slice from the same volume. Here, by showing the distribution of MgO^{+} and Mg_2O^{+} ions together, the impact of slight oxidation during sample preparation is evident. The contamination of the ball-milled powder by Fe, Cr and Ni, which is also evident in the APT mass spectra, was caused by the use of stainless steel balls (SUS304) and jars made of X46Cr13 in the ball-milling process (Supplementary Figure S2, S4). Most of the Mg-rich domains are characterized by a flat and flaky appearance, and appear to be connected to each other. These features have been observed in ball-milled metallic powders that underwent cyclic deformation and cold rolling by mechanical impact in immiscible systems like Fe−Cu [31] or Cu−Co [32]. The Mg−Mn system studied here is also immiscible, with a positive enthalpy for mixing at ΔH = +10 kJ mol^{-1} [33]. However, it is also anticipated that treatment by ball milling results in the modulated intermixing of the immiscible atoms to some extent.

(Figure 1)

The iso-concentration surfaces (isosurface) of 25 at.% Mg in the H-loaded specimen and a concentration profile through the isosurface are shown in Figure 2. Figure 2(a) clearly shows the highly inhomogeneous distribution of Mg. A light-blue cylinder with a diameter of 5 nm is placed across one isosurface and its concentration profile within the volume is plotted in Figure 2(b). The maximum Mg concentration in the Mg-rich domain with a thickness of ~5 nm was found to be approximately 40 ~ 50 at.%. This is a significant deviation from the nominal composition of $Mg_{0.25}Mn_{0.75}$. Even though the dissolution of Mg/MgH_2 into Mn was not implied by the results of the XRD analysis reported in Ref [12], our APT results confirm that the intermixing of Mg and

Mn atoms did in fact take place around the boundary of Mg-rich domains/Mn-rich matrix, reaching up to ~15 at.% Mg in the Mn-rich side on a nanometer scale. It may be that this discrepancy was due to the heavy lattice distortion induced by the ball milling process: that is, intermixing may have made it impossible for the XRD to detect the peak shift. According to the results of the APT, the size of the segregated Mg-rich domain ranged from several to several tens of nm, which is comparable to the 8-9 nm crystallite found in the Mg-rich domains (15-17 nm for the Mn-rich matrix) reported in our previous study on $Mg_{0.25}Mn_{0.75}$–D [12].

(Figure 2)

The density distribution of H^+ and H_2^+ ions detected in a volume (Figure 1(b)) is shown in Figure 3 as color maps together with Mg ions. The correlation between Mg and H-species is not clearly seen here. This strongly suggests that the observed H^+ and H_2^+ ions do not originate from MgH_2, but stem mainly from residual H/H_2 in the APT analysis chamber. Also, this hints that the loaded H in the specimen could have been desorbed before the analysis was carried out during sample transfer and pumping under UHV. This H desorption would have been enhanced had MgH_2 been destabilized. It is widely accepted that the detection of H in solid materials by the APT is mainly be attributed to this type of residual hydrogen: for this reason the use of D has been strongly recommended [23,34,35]. Therefore, the D-loaded specimen was also analyzed, as shown in the next section.

(Figure 3)

The APT results of the D-loaded specimen ($Mg_{0.25}Mn_{0.75}$–D) are shown in Figure 4. The morphological appearance of the Mg-rich domains is flat like that of the H-loaded specimen (Figure 1). It is also evident that the D-loaded specimen underwent partial oxidation, especially in the Mg-enriched areas. However, as described in the Materials and Methods section, we carried out the APT analysis without adhering to the recommendations for O_2-free transfer. The results of the H-loaded specimen in this study suggest that the D may have been desorbed from the specimen before the APT analysis even though it is likely that D was enriched in the Mg-rich domains rather than in the Mn-rich matrix.

(Figure 4)

Indeed, the density distribution shown in Figure 5 does not clearly indicate that the Mg-rich domains were D/D_2-enriched. It should be noted that the number of D_2 ions was not sufficient to extract any meaningful insight into this specimen (see also the mass spectrum, Supplementary Figure S3). The H^+ color map (Figure 5(a)) and D^+ and H_2^+ color map (Figure 5(b)) provide different impression from those of the H-loaded specimen (Figure 3): neither of the maps indicates a similar trend for the distribution of H/D. Region A in Figure 5(b) shows the enrichment of Mg as well as that of D, but without any overlapping. On the contrary, Region B suggests a spatial correlation between Mg and D. As shown in the top part of Figure 4(b), Region A is oxidized, while the oxidation of Region B is less significant (the bottom part of Figure 4(b)). Since the surface-side of the specimen is prone to oxidization after FIB treatment, the observed difference regarding the distribution of D between Region A and B might be due to the effect of the oxidized Mg, which is not likely to absorb D.

(Figure 5)

Figure 6 (a) shows a 10 nm-thick slice of the sample in Figure 4(b). A light-blue cylinder volume with a diameter of 5 nm is placed at the less oxidized region, as confirmed in Figure 5(b), and its concentration profile within this volume is shown in Figure 6(b). The Mg concentration in the Mg-rich domain with a thickness of ~10 nm was almost 50 at.%, which is similar to that of the H-loaded specimen (Figure 2). The theoretical D content (D/M) of $Mg_{0.50}Mn_{0.50}$ is 1.00 D/M, simply assuming Mg forms MgD_2. However, even though this particular region seems to be free from oxidation, the observed D content was less than 2% of this value (0.01 – 0.02 D/M). Similar to the H-loaded specimen, this result for the D-loaded specimen suggests that D was desorbed before the APT analysis, which implies the reported destabilization effect of MgD_2 accompanied with heavy lattice distortion in this nanocomposite [12].

(Figure 6)

In order to investigate the local distribution of D more in detail, we focused on the MgD_2^{2+} ions which appear at m/e = 14 – 15 in the mass spectra. Figure 7 shows 3D distribution of MgD_2^{2+} ions in the D-loaded specimen. The isosurfaces (shown as green surfaces) are implemented in the figure for better visibility of the Mg-rich domains. Interestingly, the enrichment of MgD_2^{2+} ions

was greater at the upper Mn-rich side in the boundary of Mg-rich domains/Mn-rich matrix. This was not the case in the H-loaded specimen. The ions of m/e = 14 – 15 in the H-loaded specimen were distributed almost homogeneously, corresponding to nitrogen, since MgH_2^{2+} ions should appear at m/e = 13 – 14 (Supplementary Figure S5). The light-blue cylinders A and B were chosen from nearly oxidation-free regions of different slices of yz and xz planes, respectively. In cylinder A, the Mg-rich domain, depicted by the isosurface was ~4 nm in thickness. In cylinder B, the Mg-rich domain is slightly thicker, extending to ~8 nm. The 2D density maps of MgD_2^{2+} ions are also shown in each cylinder volume to guide the eyes. It is evident that MgD_2^{2+} ions are enriched at the upper side of the Mg-rich domains: the number of MgD_2^{2+} ions shown in the maps was deconvoluted into each contribution of one Mg atom and two D atoms separately. The D concentration profile was calculated from the contribution of both of MgD_2^{2+} and D^+ (and H_2^+) ions, i.e. $(D^+ + H_2^+)/(Mg + Mn)$, as shown at the right-hand side of Figure 7. Clearly, D is enriched along the isosurfaces, reaching at 0.01 – 0.02 $(D^+ + H_2^+)/(Mg + Mn)$. According to the P (pressure) −C (composition) isotherms of $Mg_{0.25}Mn_{0.75}$−D reported in Ref [12], the D content of 0.01-0.02 D/M corresponds to the solid solution phase and also to the equilibrium D_2 pressure of ~1×10^4 Pa in the desorption process. Although the equilibrium D_2 pressure at moderate temperatures is unknown, most D should be desorbed from the Mg-rich domains under UHV condition (~2×10^{-9} Pa) in the present APT analysis, which strongly suggests that the D content in the specimen may be lower than 0.01-0.02 D/M. The APT adopted in this condition clearly leads to a D concentration profile which has hardly any D in the middle part of the Mg-rich domains, as shown in Figure 7.

(Figure 7)

It has been reported that H, and therefore D as well, is trapped at defects like grain boundaries, dislocations, and vacancies [36–38]. Incoherent or semi-coherent interfaces/boundaries are often characterized by misfit dislocations [39]. Even though the size of Mg-rich domains observed in this study is very small (4~10 nm), the unit cell volume between MgD_2 (0.061 nm^3) and Mn (0.708 nm^3) differ significantly[13], which would provide ample space for the introduction of misfit dislocations could be introduced. The cycling of H/D absorption and desorption may also result in the introduction of both of dislocations and vacancies [40]. We therefore attribute the origin of the D enrichment at the boundary of Mg-rich domains/Mn-rich matrix to the trapping effect by dislocations and/or vacancies together with heavy lattice distortion. Indeed, the contribution of

H_2 ions as a “noise” to D ions cannot be excluded since their mass-to-charge ratio is the same. In the case of the H-loaded specimen, the number ratio of H_2^+/H^+ was 0.35. If we assume the same fraction as that of the D-loaded specimen and apply it to the observed D concentration profile (Fig. 7) as a constant, the upper limit of D concentration is reduced to (1-0.35) × 0.02 (D/M) = 0.013 D/M. This value of D/M does not exclude the trace of the trapping of D, which indicates D was trapped around the boundaries.

We confirmed that the D enrichment occurred at the boundary of Mg-rich domains/Mn-rich matrix along the axis of the analysis direction (z direction), but not at the lateral side of the Mg-rich domains (Supplementary Figure S6). This could be due to the fact that D desorption via D diffusion occurred predominantly in the analysis direction. When the APT analysis temperature is increased (e.g. by a laser pulse), the diffusion of D is enhanced towards the fresh surface created during the field evaporation. For this reason, the specimen temperature should be kept below 30 K, for example, in the case of D in V [41]. In the present study, the analysis temperature was 27 K, and was kept below this reference value. However, the present analysis was carried out in laser pulsing mode, and the corresponding temperature rise of the specimen by laser irradiation [42–44] could not be avoided. Increasing the specimen temperature gives rise to a “tail” of D profile, as has been reported in an earlier study [23]. The concentration of the observed local enrichment of MgD_2 at the upper side of the Mg-rich domain (Figure 7) could be due to this temperature effect, resulting in a thermo-migration. That is, it could be that D gradually diffuses along the z direction by decomposing MgD_2 phase. However, D atoms are trapped around the boundary of Mg-rich domains/Mn-rich matrix, where defects are induced with heavy lattice distortion. To fully confirm the concentration of the trapped D, in our previous work, the activation energy for diffusion of hydrogen E_d in $Mg_{0.25}Mn_{0.75}$–H was estimated to be 86.0 kJ mol^{-1} [13], which is significantly higher than that of E_d = 24.1 kJ mol^{-1} for bulk Mg–H [45]. This large difference of E_d suggests the slow mobility of H(D) in $Mg_{0.25}Mn_{0.75}$–H(D), and explains the results of the APT observation in this study well. The distortion of the crystal lattice destabilizes the hydride phase, and also induces trapping effect of H(D) by the large distribution of the site energies for H(D) [46].

Conclusions

An APT analysis of Mg–Mn nanocomposites loaded with H and D was successfully conducted. The results show that the Mg-rich domains were several to 10 nm in thickness. The morphology

of the domains was not spherical, as has been speculated on the basis of earlier TEM observations, but rather deformed, resulting in interconnected Mg-rich domains embedded in a Mn-rich matrix. This complex morphology was attributed to the ball milling treatment. Lattice distortion, which is a primary origin of the destabilization of $MgH(D)_2$, is heavily induced around the Mg-rich domains. Our APT investigation revealed that D is enriched at the boundary of the Mg-rich domains/Mn-rich matrix, but not significantly in the middle of the Mg-rich domains. The heavy lattice distortion in the Mg-rich domains destabilizes both $MgH(D)_2$ and the lattice defects induced at the boundary facing a Mn-rich matrix trap H(D), resulting in the retarded diffusion of H(D).

Figure captions

Fig. 1 APT ion maps of H-loaded specimen ($Mg_{0.25}Mn_{0.75}$−H) separately showing (a) Mg (green) and Mn (purple) and (b) H (light blue), H_2 (yellow), Mg (green) and MgO or Mg_2O (dark blue sphere). Displayed fraction of ions is 100% for all ions. Mg-rich domains are inhomogeneously distributed and embedded in the Mn-rich matrix.

Fig. 2 Distribution of Mg in the H-loaded specimen ($Mg_{0.25}Mn_{0.75}$−H). (a) Iso-concentration surfaces of 25 at.% Mg. Green dots represent Mg ions. Light-blue cylinder with a diameter of 5 nm indicates the position of concentration profile in (b). (b) 1-dimentional concentration profile in the cylinder shown in (a). Corresponding ion map of Mg and Mn is shown together with the profile.

Fig. 3 Distribution of hydrogen and Mg in the H-loaded specimen ($Mg_{0.25}Mn_{0.75}$−H) taken from a slice 10 nm in thickness in the xz-plane. (a) 2-dimensional density map of H^+ ions and ion distribution map of Mg (green) ions. (b) 2-dimensional density map of H_2^+ ions and ion distribution map of Mg (green) ions. Note that density distribution of H^+ and H_2^+ is similar.

Fig. 4 APT ion maps of D-loaded specimen ($Mg_{0.25}Mn_{0.75}$−D) separately showing (a) Mg (green) and Mn (purple) and (b) H (light blue), D or H_2 (yellow), D_2 (red sphere), Mg (green) and MgO or Mg_2O (dark blue sphere). Displayed fraction of ions is 100% for all ions. Note that, like the H-loaded specimen, the Mg-rich domains are inhomogenously distributed.

Fig. 5 Distribution of hydrogen and Mg in the D-loaded specimen ($Mg_{0.25}Mn_{0.75}$−D) taken from a slice with a thickness of 10 nm in xz-plane. (a) 2-dimensional density map of D^+ ions and ion distribution map of Mg (green) ions. (b) 2-dimensional density map of D_2^+ ions and ion distribution map of Mg (green) ions. Region A shows poor correlation between Mg and D^+ or H_2^+, while a correlative relationship is visible in Region B.

Fig. 6 Distribution of ions in D-loaded specimen ($Mg_{0.25}Mn_{0.75}$−D) taken from a slice with a thickness of 10 nm in the xz-plane. (a) D_2 (red sphere), D or H_2 (yellow sphere), Mg (green) and MgO or Mg_2O (dark blue sphere). Light-blue cylinder with a diameter of 5 nm indicates the position of concentration profile in (b). (b) 1-dimentional concentration profile in the cylinder shown in (a). Corresponding ion map of D or H_2, Mg and Mn is shown together at the top of profile.

Fig. 7 D-loaded specimen ($Mg_{0.25}Mn_{0.75}$−D) representing MgD_2 ions (blue sphere) and iso-concentration surface of 25at.% Mg (green). A yz-plane slice and an xz-plane slice, with a thickness of 10 nm, is cropped from the original map, respectively. Cylinders A and B (in light-blue color, 5 nm-diameter) are placed across a Mg-rich domain, respectively in the yz-plane or in the xz-plane, and the ion distribution of Mg (green sphere), MgD_2 (blue sphere), D or H_2 (yellow sphere) and D_2 (red sphere) is displayed. The 2-dimensional density map of the MgD_2 ions in the same cylinder is shown together. The 1-dimensional concentration profile of D and H_2 ions in each cylinder volume is plotted at the right-hand side of the figure (see text for details).

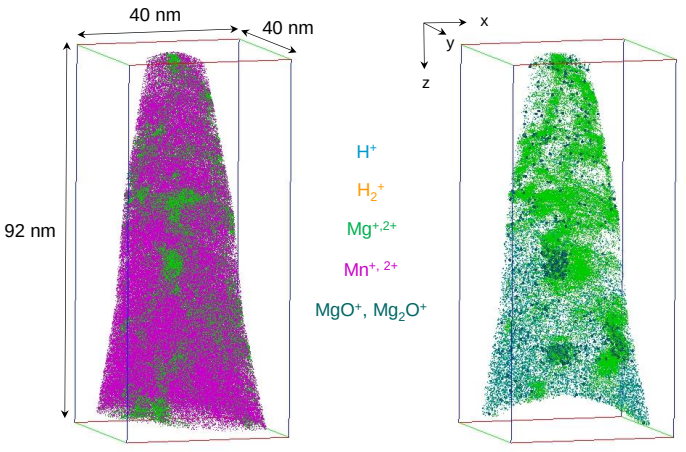
40 nm
40 nm
92 nm
x
y
z
H+
H2+
Mg+,2+
Mn+, 2+
MgO+, Mg2O+
(a)
(b)

Fig. 1

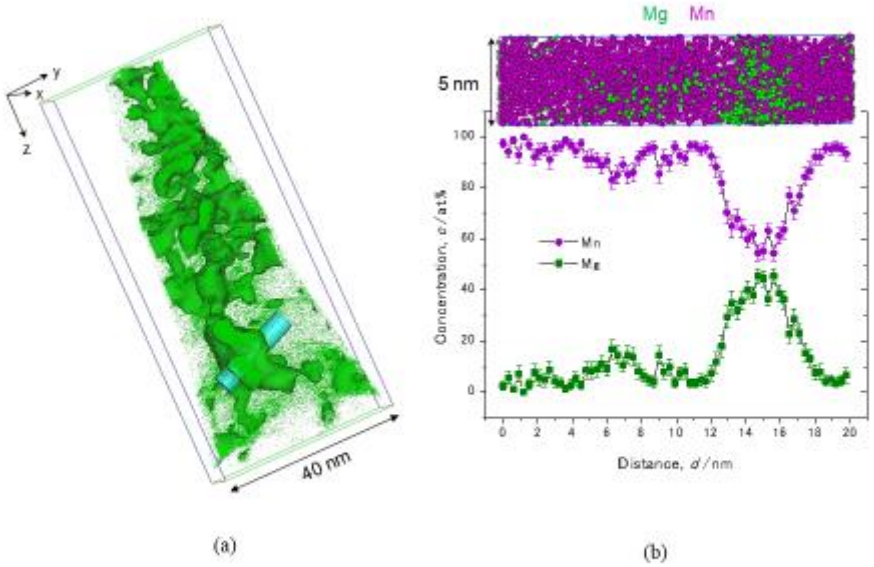
y
x
z
40 nm
Mg
Mn
5 nm
Mn
Mg
Concentration, c / at%
Distance, d / nm
(a)
(b)

Fig. 2

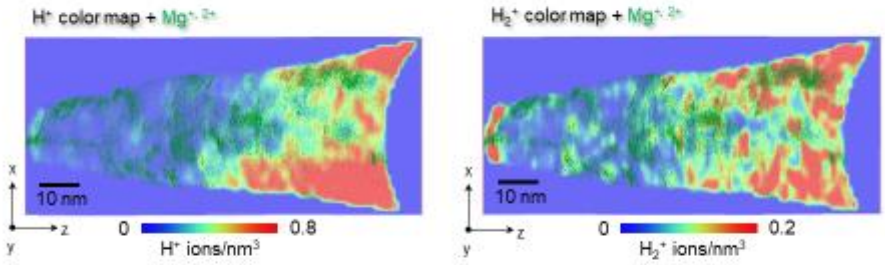

(a) (b)

Fig. 3

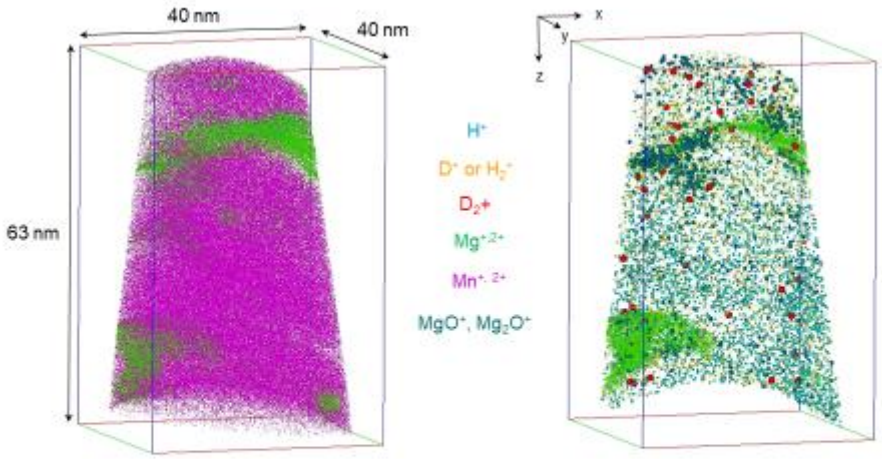

(a) (b)

Fig. 4

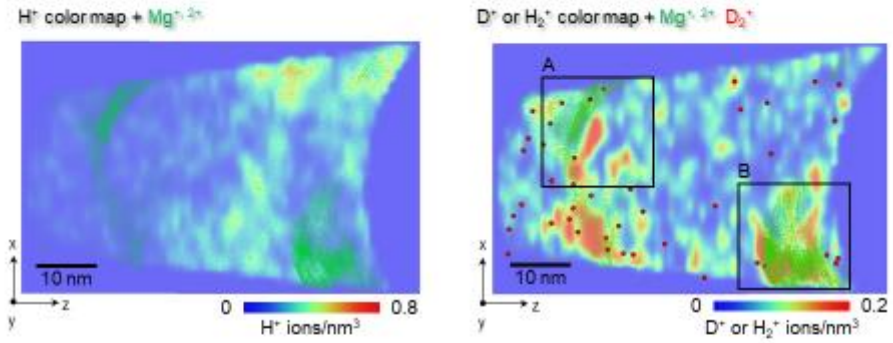

(a) (b)

Fig. 5

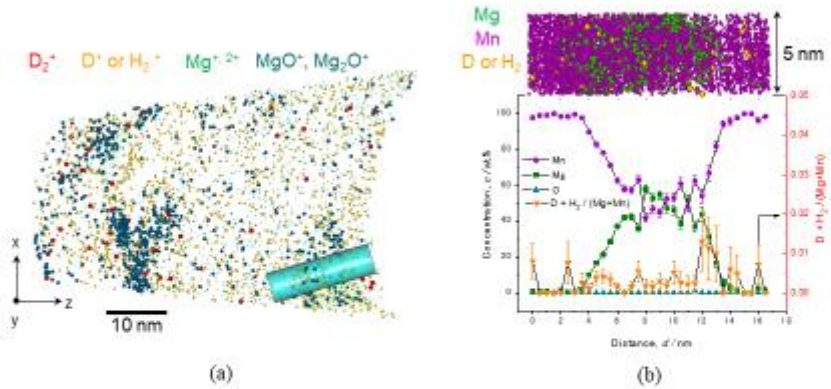

(a) (b)

Fig. 6

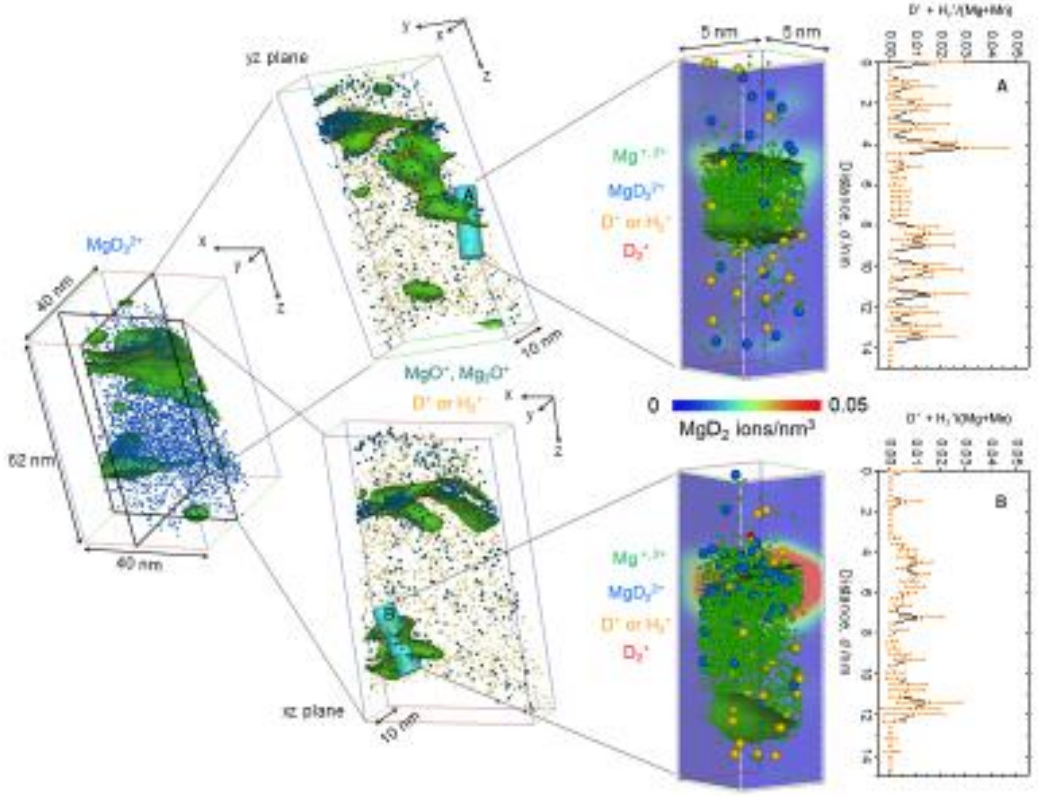
yz plane
xz plane
MgD2 2+
40 nm
62 nm
40 nm
10 nm
10 nm
MgO+, Mg2O+
D+ or H2+
5 nm
5 nm
Mg+, 2+
MgD2 2+
D+ or H2+
D2+
0
0.05
MgD2 ions/nm3
Distance, d (nm)
A
B

Fig. 7

Supplementary Information

SEM image of the prepared tip by FIB

Figure S1 shows a typical Secondary Electron Microscope (SEM) image of the finalized tip prepared by Focused Ion Beam (FIB). The tip was prepared from D-charged specimen. Sharp needle-like tip shape verifies successful tip preparation.

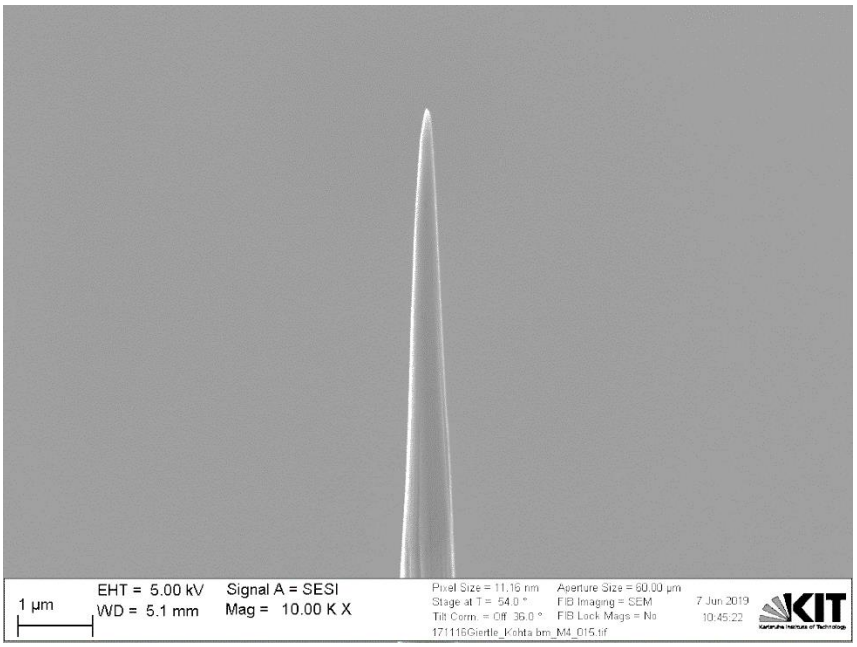

Figure S1 SEM image of an APT tip prepared from D-charged specimen

Atom probe mass spectra of H-loaded and D-loaded specimens

Figure S2 shows atom probe mass spectrum of H-loaded specimen ($Mg_{0.25}Mn_{0.75}$−H). Observed Fe, Cr could be contaminants from milling jar made of X46Cr13. Similarly, Ni could originate from SUS304 balls. The ratio of the detected ions being Fe/(Cr+Ni) = 2.7 suggests that the majority of contamination is SUS304 component. N^+ peaks were observed at m/e = 14 and at m/e = 15. These peaks might overlap if MgD_2^+ ions are present in D-loaded specimen.

Figure S3 shows atom probe mass spectrum of D-loaded specimen ($Mg_{0.25}Mn_{0.75}$−D). The trend is similar to that of the H-loaded specimen. However, the presence of D_2^+ verifies that certain amount of D is present in the specimen, as discussed in the Results and discussion section. Distribution of Fe, Cr and Ni is shown in Figure S4. Slight enrichment of Ni was found especially

where oxidation was visible. We have omitted corresponding enriched area to investigate D distribution.

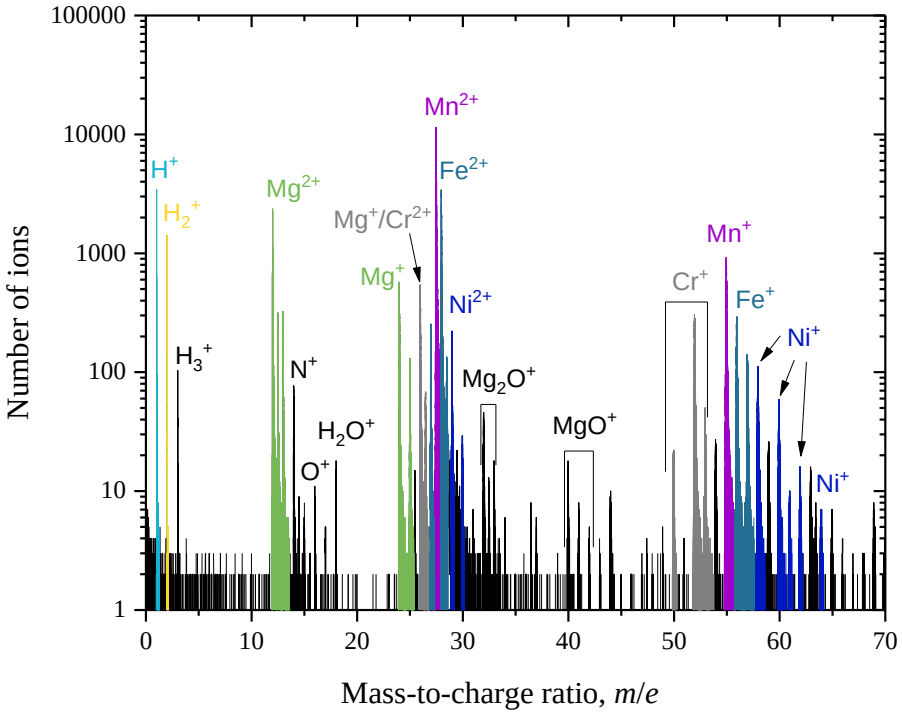

Figure S2 Atom probe mass spectrum of H-loaded specimen.

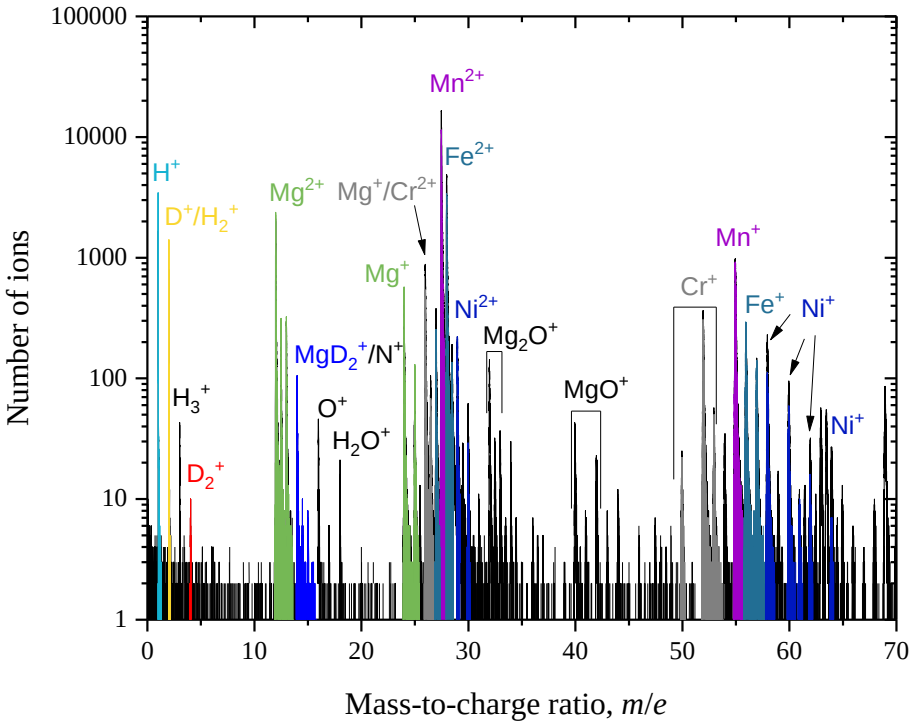

Figure S3 Atom probe mass spectrum of D-loaded specimen.

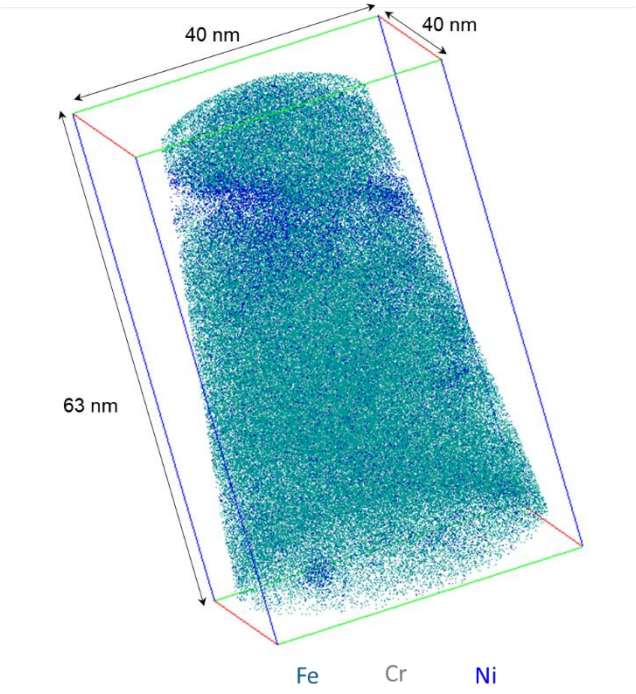

Figure S4 Distribution of Fe, Cr and Ni ions in D-loaded specimen.

Distribution of ions at m/e = 14–15

When considering possible contribution of MgD_2^+ (m/e = 14, 14.5, 15) to total D concentration, we should be cautious on the overlap of N^+ (m/e = 14, 15) appearing at the same mass window. In case of MgH_2 (m/e = 13, 13.5, 14), there is also an overlap with N^+ at m/e = 14. Distribution of ions at m/e = 14 – 15 in the H-loaded and D-loaded specimens is compared in Figure S5. Blue spheres represent the position of ions appearing at m/e = 14 – 15. Regions within green surfaces show where the Mg concentration is higher than 25 at.%. It is clearly seen that the blue spheres are not enriched in the H-loaded specimen (Fig. S5 (a)). This suggests that these ions are mostly N^+, but not MgH_2. Most probably, significant H desorption occurred before/during the APT analysis, and MgH_2-enrichment, if any, is not visible. Note that the desorption of H occurs quicker than that of D due to the difference in diffusion coefficients (mass effect).

In case of the D-loaded specimen, it is obvious that the blue spheres, suggesting MgD_2^+, are enriched at the vicinity of Mg-rich domain, at the bottom of map (Fig. S5 (b)). As the upper part of this specimen was severely oxidized as described in the Results and discussion section, it is rationalized to discard this region and to focus on less oxidized region (the bottom part of map in Fig. S5(b)). This is supported also by the enrichment of ions at m/e = 2 at the same region (see also Figure 5(b) color map in the main text).

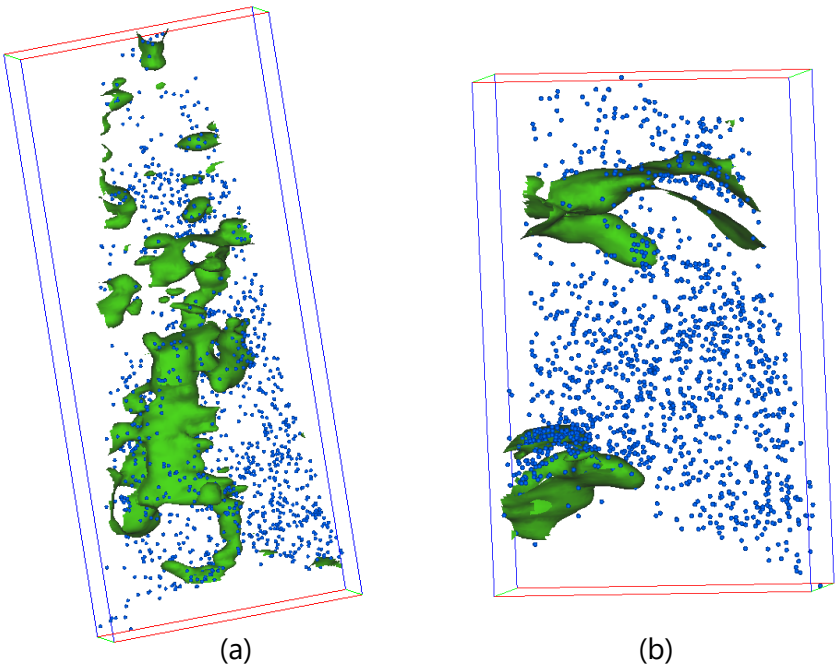

Figure S5 3D maps of ions at m/e = 14-15 in (a) H-loaded and (b) D-loaded specimens. Both maps are slices of xz-plane with a thickness of 10 nm. Blue spheres represent the position of ions within mass range of m/e = 14-15. Green surfaces depict iso-concentration surface of 25 at.% Mg.

Lateral and vertical distributions of ions at m/e = 2

We have carefully investigated the distribution of ions with a mass-to-charge ratio of m/e = 2, namely H_2 and D to interpret our results. Figure S6 (a) and (b) compares both the lateral and vertical distribution of ions at m/e = 2 (H_2 and D) in the specimen. Here, a cube with a volume of 10 nm x 10 nm x 10 nm (light blue cube at the left-hand side) was first cropped from the entire volume containing Mg-rich region. In this volume, iso-concentration surfaces of Mg (Mg 25 at.%) and iso-density surfaces of D^+ or H_2^+ ions (0.5 ions/nm^3) are shown together. Out of this cube, slices of yz- or yx-plane with a thickness of 5 nm was cropped separately and the density of Mg is displayed as a color map (number of Mg ions/nm^3). Dark yellow spheres indicate the location

of D^+ or H_2^+ ions in each slice. Comparison of Fig. S6 (a) and (b) clearly shows us that there are D^+ ions remaining in the D-loaded specimen. Moreover, these D^+ ions are observed at the vicinity of the Mg-rich domains along the axis of analysis direction (z direction), but not at the lateral side of the Mg-rich domains (compare yz and yx planes in Fig. S6 (b)). This suggests surface segregation (desorption) of D probably during the analysis.

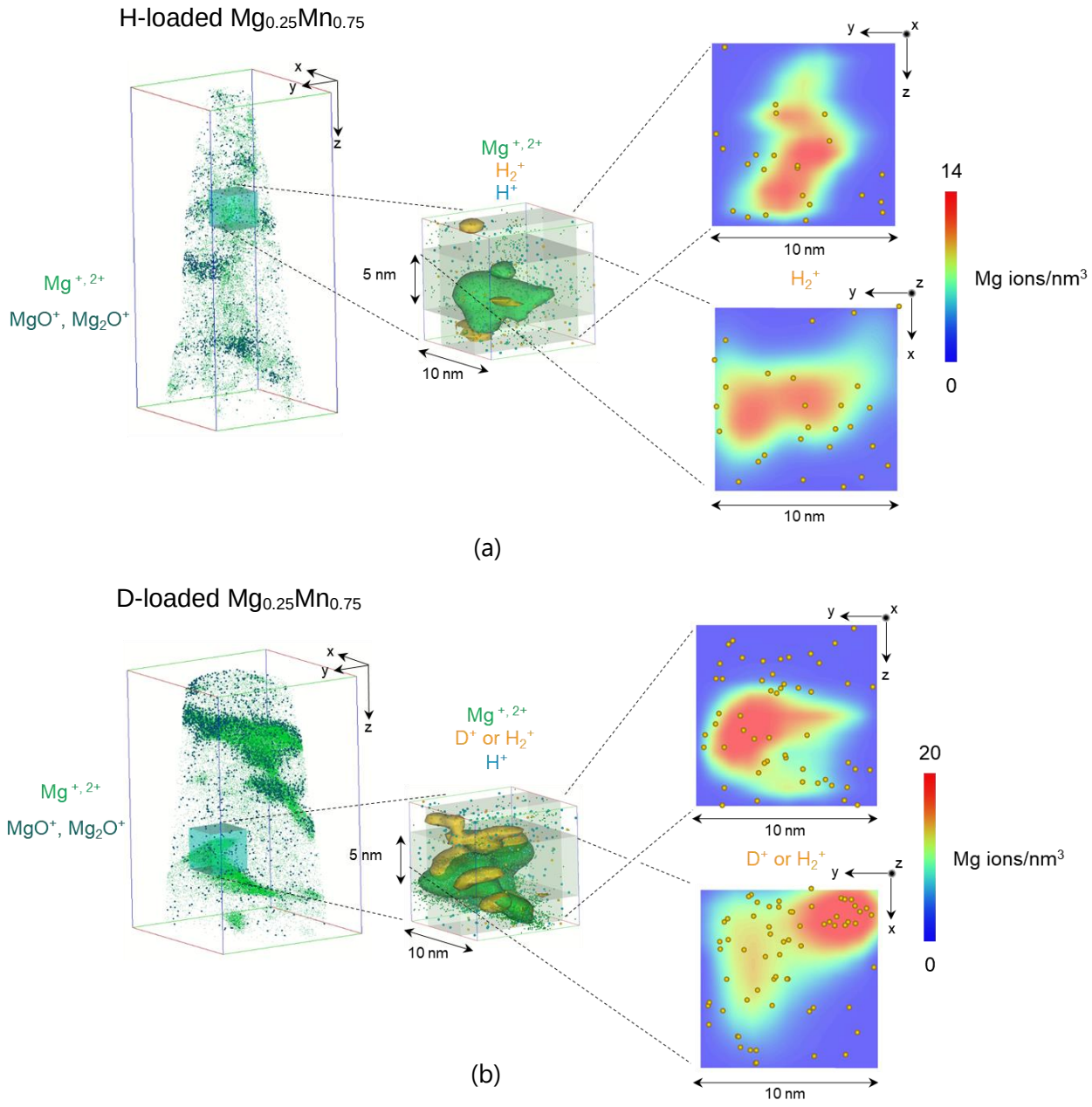

Figure S6 Comparison of ion distribution in (a) H-loaded and (b) D-loaded specimens. Iso-concentration surfaces of Mg (25 at.% Mg) and iso-density surfaces of D^+ or H_2^+ ions (0.5 ions/nm^3) are shown together in a light blue cube of each 3D ion map. Out of this cube, each 2D contour color map in yz- or yx-plane (5-nm thick) is cropped and displayed density distribution of Mg ions (number of ions/nm^3), on which the distribution of D^+ or H_2^+ ions is superimposed.